Influence of dopant size and doping method on the structure and thermoelectric properties of PBTTT films doped with F 6 TCNNQ and F 4 TCNQ

Vishnu Vijayakumar, Pablo Durand, Huiyan Zeng, Viktoriia Untilova, Laurent Herrmann, Patrick Algayer, Nicolas Leclerc, Martin Brinkmann

Influence of dopant size and doping method on the structure and thermoelectric properties of PBTTT films doped with F_6TCNNQ and F_4TCNQ

Vishnu Vijayakumar[1], Pablo Durand[2], Huiyan Zeng[1], Viktoriia Untilova[1], Laurent Herrmann[1], Patrick Algayer[1], Nicolas Leclerc[2*], Martin Brinkmann[1*]

(1) Université de Strasbourg, CNRS, ICS UPR 22, F-67000 Strasbourg, France

(2) Université de Strasbourg, CNRS, ICPEES UMR 7515, F-67087 Strasbourg, France

Corresp. Authors : martin.brinkmann@ics-cnrs.unistra.fr

leclercn@unistra.fr

Abstract

Doped polymer semiconductors are ideal candidates to capture waste heat in ambient conditions using modest temperature gradients close to room temperature. Mastering the doping mechanism of polymer semiconductors is therefore crucial to enhance the performances of these materials. This study focuses on the structure-property correlations in oriented films of poly(2,5-bis(3-dodecyl-2-thienyl)thieno[3,2-*b*]thiophene) (C_{12}-PBTTT) doped with 1,3,4,5,7,8-Hexafluoro-tetracyanonaphthoquinodimethane (F_6TCNNQ) and 2,3,5,6-tetrafluoro-7,7,8,8-tetracyano-quinodimethane (F_4TCNQ). Slower diffusion of the larger F_6TCNNQ molecules in PBTTT crystals results in a better ordering upon intercalation in the layers of alkyl side chains as compared to F_4TCNQ. Both, the higher degree of polymer chain oxidation and ordering of F_6TCNNQ- dopants in the C_{12}-PBTTT crystals accounts for the improved electrical conductivity and thermoelectric properties. A new doping protocol called "incremental concentration doping" leads to electrical conductivities of up to 2400 S/cm and thermoelectric power factors of 530±200 $\mu Wm^{-1}K^{-2}$ in aligned C_{12}-PBTTT doped with F_6TCNNQ. The progressive intercalation of dopants helps preserve the high level of order initially present in the aligned C_{12}-PBTTT films, hence, to reach higher charge mobilities. The correlations between thermopower S and charge conductivity σ measured parallel and perpendicular to the polythiophene chain follow two master curves regardless of the chemical

nature of the dopant: $S \propto \sigma^{-1/4}$ along the chain direction whereas $S \propto -\ln(\sigma)$ perpendicular to the chains.

1. Introduction

Conducting polymers are of central interest in plastic electronics not only for their charge transport properties used for instance in polymer injection layers using for instance poly(3,4-ethylenedioxythiophene)/poly(styrenesulfonate) (PEDOT: PSS) but also for their interesting thermoelectric (TE) properties. [1] TE properties of conducting polymers depend on several quantities such as their charge conductivity σ, their Seebeck coefficient S and their thermal conductivity κ. Ideally, a good TE material should have high σ and S and low κ. Since the measure of κ is difficult, the performance of TE materials is often quantified by their power factor $PF=\sigma S^2$. Several studies on doped polythiophenes have shown that the power factor PF scales with the charge conductivity such as $PF \propto \sqrt{\sigma}$. This is why a common strategy to enhance TE properties of polymers is to maximize their charge conductivity i.e. the charge mobility and the charge carrier density, while keeping κ to a minimum.

Doping is a well-known method to transform polymer semi-conductors (PSCs) such as regioregular poly(3-hexylthiophene) or PBTTT into conducting ones.[2–6] P-type doping of PSC is readily performed by using acceptor molecules such as 2,3,5,6-tetrafluoro-7,7,8,8-tetracyanoquinodimethane (F_4TCNQ) that can withdraw an electron from the PSC and create positively-charged polarons on the polymer backbone. Various groups have focused on the doping method as a handle to reach improved TE performances in doped polymer semiconductor films.[7–12]

Sequential doping, i.e. the doping of a highly crystalline PSC film with a dopant solution in an orthogonal solvent is an effective method to enhance the TE properties as compared to direct mixing of polymer and dopant in a common solvent.[9,10,13,14] Vapor phase doping leads to even higher charge conductivities as it preserves order along the chain direction in the doped polymer crystals. As demonstrated in previous studies, dopants such as F_4TCNQ are mainly intercalated in the layers of alkyl side chains of the polymers[15,16] and the highest possible doping level depends on the length and packing of alkyl side chains. [16] The final thermoelectric properties of the doped films can further be enhanced if the films are oriented. [14-16] Both, thermopower and charge conductivity are augmented in aligned P3HT and PBTTT films along the chain direction, making it possible to improve substantially the TE power factor of the layers.

The choice of the dopant is also of paramount importance. The LUMO level of the acceptor molecules must be well situated with respect to the HOMO of the p-type polymer. The high electrical conductivity observed in F_4TCNQ doped polythiophenes relates to the favorable energetic offset between the HOMO of the polymer and the LUMO of F_4TCNQ. For instance, the HOMO of P3HT and PBTTT is in the range -4.8 eV to - 5.2 eV *versus* -5.24 eV for the LUMO of F_4TCNQ (see Figure 1). Besides F_4TCNQ, stronger inorganic dopants such as I_2 and $FeCl_3$ have also been used with P3HT and PBTTT. [17, 18] Doping aligned films of C_{12}-PBTTT with $FeCl_3$ leads to very high conductivities of the order of 10^5 S/cm.[15] However, $FeCl_3$ and I_2 are difficult to use because of both their high instability in air and corrosive nature. [19,20] In this perspective, the electron-deficient molecular dopant 1,3,4,5,7,8-Hexafluoro-tetracyanonaphthoquinodimethane (F_6TCNNQ) (see figure 1) is particularly appealing.[21,22] Karpov and co-workers showed that doping P3HT with F_6TCNNQ allows to reach charge conductivities of 7 S/cm i.e. larger than for F_4TCNQ doping. [22] The improved electrical conductivity was attributed to a combination of higher charge carrier mobilities and higher doping strength (LUMO at -5.37 eV for F_6TCNNQ *versus* -5.24 eV for F_4TCNQ) leading to a higher charge carrier concentration. Moreover, integer charge transfer between P3HT and F_6TCNNQ was demonstrated. [23]

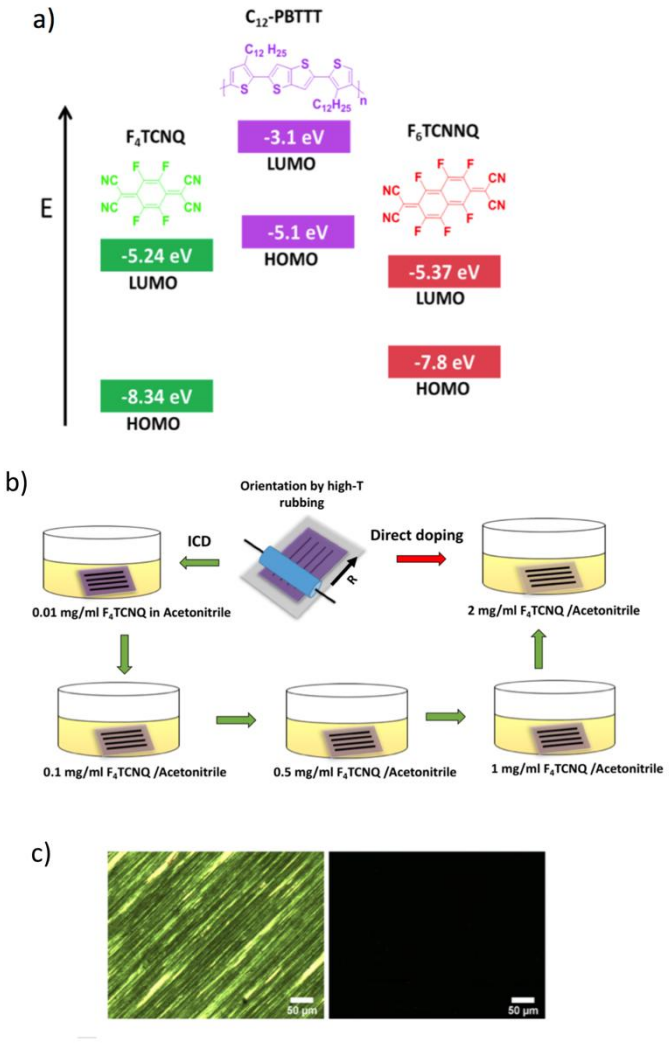

Figure 1. *A) Schematic representation of HOMO and LUMO levels F_4TCNQ, F_6TCNNQ and C_{12}-PBTTT. B) Two-step preparation of highly oriented and crystalline C_{12}-PBTTT films. Schematic illustration of incremental concentration doping (ICD) and direct doping (DD). The first step consists of chain alignment and crystallization by high-T rubbing followed by sequential doping in solutions of F_4TCNQ or F_6TCNNQ in acetonitrile. ICD implies doping the same sample with solutions of increasing concentration whereas for DD, the sample is directly doped at a high concentration. C) Polarized optical microscopic images of F_6TCNNQ doped C_{12}-PBTTT using the ICD method and showing high*

birefringence (T_R =125 °C , film doped up to C_{F4TCNQ}= 1mg/ml) i.e. preservation of alignment after doping.

Given the proposed context and state-of-the-art, the present contribution aims at investigating the following important issues. First, we want to know to what extent the doping of C_{12}-PBTTT with F_6TCNNQ differs from that with F_4TCNQ in terms of structure, doping kinetics and resulting TE properties. We will also determine how the intercalation of F_4TCNQ in the layers of alkyl side chains of C_{12}-PBTTT compares with that of F_6TCNNQ. Importantly, we will investigate the relationship between the degree of order of the dopant anions in the PSC and the resulting electrical conductivities.

To answer these issues, we have chosen C_{12}-PBTTT as a model PSC (see Figure 1). This polymer is readily aligned by high-temperature rubbing leading to dichroic ratio beyond 15. [24,25] Polarized UV-Vis-NIR spectroscopy and low dose electron diffraction have been used to uncover the location and orientation of the dopant anions in the side chain layers of C_{12}-PBTTT. Polarized UV-Vis-NIR spectroscopy helped determine the correlations between the orientation of the dopant anions and the polythiophene backbones. Polarized UV-vis-NIR spectroscopy has been used to measure the diffusion kinetics of both F_4TCNQ and F_6TCNNQ into the layers of the interdigitated alkyl side chains of C_{12}-PBTTT. [16]

Finally, a new protocol for sequential doping called incremental concentration doping (ICD) is introduced with the objective to intercalate dopant molecules in a progressive manner in the structure of C_{12}-PBTTT. The changes in the crystal structure of the thin films were followed by low dose electron diffraction. Promising thermoelectric performances are observed record conductivities of 2430±500 S/cm and PF=530 $\mu Wm^{-1}K^{-2}$.

2. Results and discussion.

2.1 Fabrication of highly oriented conducting PBTTT thin films.

It has been shown that polymers such as PBTTT can be easily oriented by rubbing at high temperature.[24,25] Based on these results, oriented C_{12}-PBTTT thin films were doped sequentially by dipping the films in acetonitrile solutions of F_4TCNQ and F_6TCNNQ, respectively (see figure 1B). The doped thin films show high levels of orientation evidenced by polarized optical microscopy (see figure 1C). Herein we introduce a new doping procedure called "incremental concentration doping" (ICD). It is a modified version of classical sequential doping (see figure 1.B). In ICD, the oriented thin films are doped by dipping a given sample successively in solutions of dopants of increasing concentration. This is different from the conventional sequential doping referred to as direct doping (DD) for which each sample is dipped a single time in a solution of given concentration. In this study, all the thin films are doped by ICD and direct doping is used as a reference.

2.2. Spectroscopic signatures of polarons and anions obtained by polarized UV-vis-NIR spectroscopy.

Let us first present the spectroscopic signatures of the two dopants and corresponding anions in solution. Both, F_4TCNQ^- and F_6TCNNQ^- anions display distinct signatures in the form of vibronic structures. In order to confirm the presence of the F_6TCNNQ^- anions in the thin films of PBTTT, a solution of pure F_6TCNNQ^- anions was prepared by reduction with ferrocene in dichloromethane, the corresponding UV-Vis-NIR spectrum is shown in figure 2 and compared to that of F_6TCNNQ. F_6TCNNQ^- shows characteristic bands at 1143, 976 and 850 nm and there are no corresponding absorption bands in that spectral range for neutral F_6TCNNQ. The latter is characterized by two bands at 481 and 454 nm that overlap partially with some bands of the F_6TCNNQ^- anion. The molar

extinction coefficient of F_6TCNNQ^- has been determined and amounts to 53700 $L{\cdot}Mol^{-1}{\cdot}cm^{-1}$ (see Figure ESI1). As seen in figure 2, the vibronic structure of the F_6TCNNQ^- anions in the doped C_{12}-PBTTT films matches quite well that of the anion in solution. There is only a small redshift in the thin films (1157 nm versus 1143 nm in solution).

Having identified the spectral signatures of the F_6TCNNQ^- anion, we can now analyze in more details the polarized UV-vis-NIR spectra of the films doped with F_6TCNNQ. As seen in Figure 3A, the polaronic bands P1 and P2 are polarized along the rubbing direction and their intensities increase with doping concentration and saturate once the concentration reaches 0.5 mg/ml. Even for very low doping concentrations such as 0.01 mg/ml, the P1 and P2 bands are present. Contrary to the polaronic bands, the absorption bands of the neutral polymer (N) decrease with increasing dopant concentration. The polarized UV-Vis-NIR spectra along the perpendicular direction are dominated by the absorption bands of the F_6TCNNQ^- anions. As observed in our previous studies,[15,16] the F_6TCNNQ^- anion bands are polarized perpendicular to the rubbing direction. This demonstrates that, both F_4TCNQ^- and F_6TCNNQ^- anions are intercalated in the layers of the interdigitated side chains of C_{12}-PBTTT.

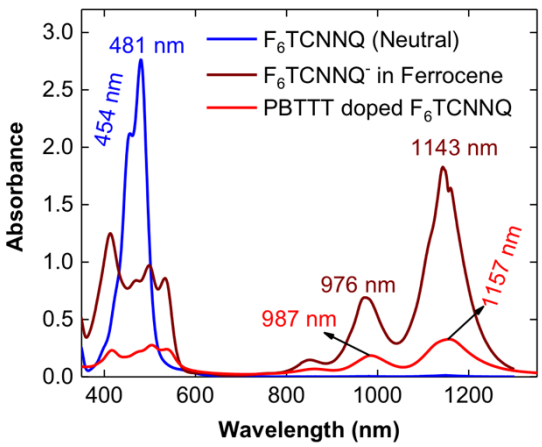

Figure 2. *Absorption in solution of neutral F_6TCNNQ (blue) andF_6TCNNQ$^-$ anion (brown) after reduction with ferrocene. The absorption of F_6TCNNQ$^-$ in thin films is shown in red.*

For both F_4TCNQ and F_6TCNNQ dopants, the intensity of the anion bands increased with doping concentration and saturates for C= 0.5-1.0 mg/ml. The polaron bands P1 and P2 show a similar saturation for POL//R. Interestingly, no absorption from the polarons is seen for POL ⊥R. In the case of P3HT, this absence has been attributed to the fact that the amorphous phase of P3HT is little doped with F_4TCNQ due to a larger offset between the amorphous polymer's HOMO and the dopant's LUMO as compared to crystalline P3HT.[26] The present results with F_6TCNNQ suggest a similar effect for C_{12}-PBTTT: F_6TCNNQ cannot dope efficiently the amorphous phase of C_{12}-PBTTT. The comparison with the study on $FeCl_3$-doped C_{12}-PBTTT further confirms this point.[14] It has been shown that $FeCl_3$ is able to dope both the amorphous and ordered phase of C_{12}-PBTTT, as inferred from the presence of the polaronic bands for POL ⊥R.

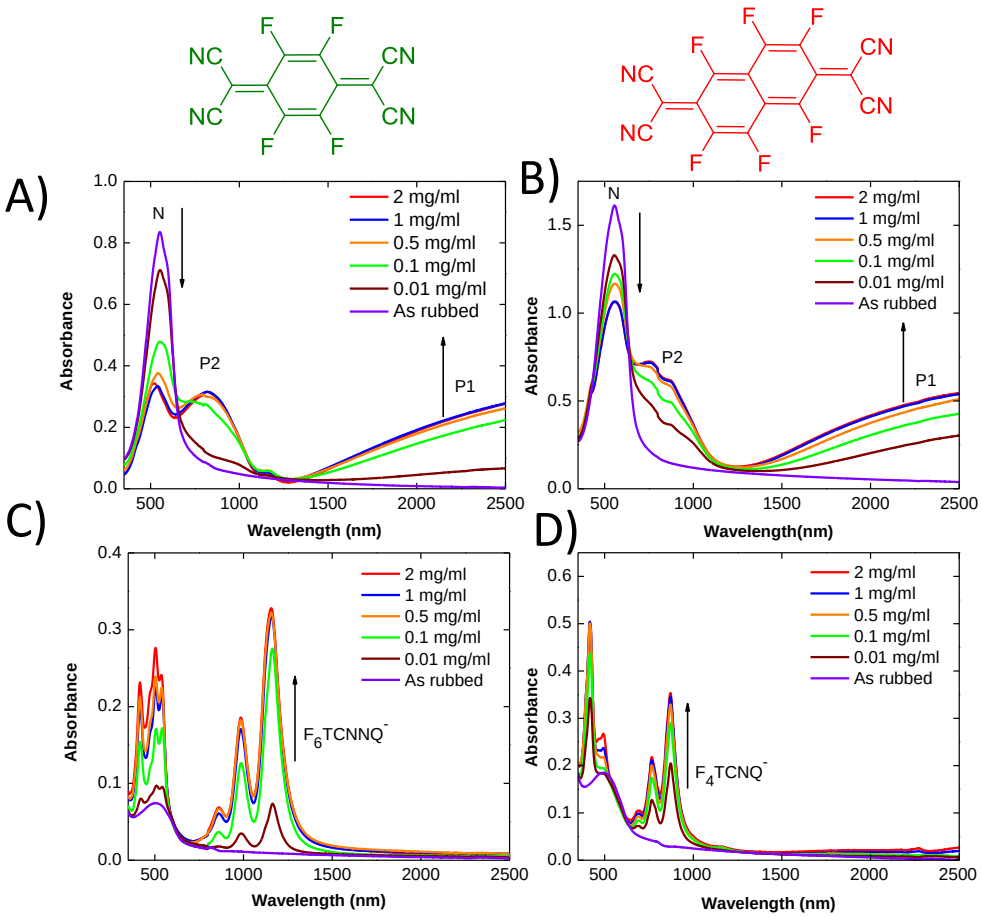

Figure 3. *A) and B) Evolution of the UV-Vis-NIR spectra of rubbed C12-PBTTT films doped with increasing concentration of F_4TCNQ for POL//R and for POL ⊥R, respectively. C) and D) Evolution of the UV-Vis-NIR spectra of rubbed C12-PBTTT films doped with increasing concentration of F_6TCNNQ for POL//R and for POL ⊥R, respectively. P1 and P2 correspond to polaronic bands of doped C_{12}-PBTTT and the neutral polymer absorption is labelled as N.*

Comparing the UV-vis-NIR spectra of F_4TCNQ and F_6TCNNQ-doped films shows differences in the apparent P1 and P2 band positions. For F_6TCNNQ, P2 is centered at 824 nm whereas for F_4TCNQ, it is centered around 780nm. The shape of the P1 bands, with the appearance of a plateau/saturation in P1 absorption in the F_4TCNQ case, suggests a similar red-shifted band position for F_6TCNNQ. The position of the polaronic bands is linked to the localization of the polarons due to Coulombic

interactions with the anions as demonstrated by Ghosh et al.[27, 28] Accordingly, the polaron seems to be more delocalized in the case of F_6TCNNQ as compared to F_4TCNQ.

Another important difference is related to the oxidation level of the PBTTT chains. Figure 3A and B show that the contribution of neutral PBTTT to the absorption is larger for the films doped with F_4TCNQ than F_6TCNNQ. The presence of remaining neutral polymer absorption (N) was attributed to the presence of undoped polymer chain segments in the doped films. A lower remaining absorbance of the neutral polymer for F_6TCNNQ indicates higher overall oxidation of C_{12}-PBTTT as compared to F_4TCNQ. This is consistent with the lower lying LUMO of F_6TCNNQ, favoring charge transfer to the PBTTT chains. Integer charge transfer between polymer and dopant is evidenced from the linear dependence between polaron and anion absorbances for both F_4TCNQ^- and F_6TCNNQ^- (see figure ESI2). Accordingly, F_6TCNNQ seems to induce a larger doping level of the polymer, hence, should induce a higher charge carrier density (vide infra).

2.3. Doping kinetics.

The fact that the UV-vis-NIR spectra for POL $\perp$ R are dominated by the absorption of the dopant anions helped determine the diffusion coefficients of the dopant anions into the layers of the alkyl side chains of the thin films. Polarized UV- Vis-NIR spectroscopy can be used to follow the time dependence of the absorbance of both F_4TCNQ^- (875 nm) and F_6TCNNQ^- (1158 nm) anions (see figure ESI3) versus doping time. [15,16] The kinetics of dopant diffusion into the C_{12}-PBTTT thin films are measured by recording the UV-vis-NIR spectra of the doped films for various doping times.

The contact time of the oriented polymer with the dopant solution is increased and the corresponding UV-Vis-NIR spectra along both perpendicular and parallel directions are recorded (see figure ESI3A-D). The signals of the dopant anions are visible even for short contact time of 5s and their intensity increases and saturate with doping time.

For short doping times, the absorption of both dopant anions scales like $\sqrt{t}$. This is an indication for a diffusion-limited doping mechanism. The saturation observed for longer doping times is due to the finite film thickness: the whole film is doped after 6-10 min (see Figure ESI3). The fact that no clear absorption of the neutral F_6TCNNQ is seen in the UV-vis-NIR spectra indicates that the time-dependence of the F_6TCNNQ^- bands reflects the diffusion of the anion rather than the diffusion of the neutral dopant into the polymer film.[16] This is consistent with the assumption of Li et al. that the rate of equilibration between the two species (neutral and ionized dopant) is much faster than the rate of diffusion i.e. the observed kinetics reflects the dopant diffusion. [29] The plot of normalized intensity of anions vs $t^{1/2}/l$ helped determine the diffusion coefficients of F_4TCNQ^- and F_6TCNNQ^- and this representation is independent of the polymer film thickness.[16] The following phenomenological equation was used to fit the absorbance of the anion as a function of the doping time:

$$A_x(t) = A_0(1 - \exp\left(-\frac{\sqrt{D}}{l}(t)^{\frac{1}{2}}\right)) \qquad (1)$$

Where A is the absorption at wavelength λ of the anion (λ = 873 nm for F_4TCNQ^- and 1158 for F_6TCNNQ^-). A_0 is the absorbance of the anion at saturation, l is the film thickness and D is the diffusion coefficient of F_4TCNQ^- or F_6TCNNQ^- in the matrix of C_{12}-PBTTT.

The larger F_6TCNNQ^- anion shows a lower 2×10^{-12} cm^2/s diffusion coefficient with respect to 9×10^{-12} cm^2/s for F_4TCNQ^- (see figure 4A). Both diffusion coefficients were close to the diffusion coefficients of iodine into the P3HT films reported by Maliakal (2.5×10^{-11} cm^2/s). [30] This result highlights the influence of the size of the dopant anion on its diffusion into the highly interdigitated side chain layers. Smaller anions such as F_4TCNQ^- can diffuse and intercalate faster into the layers of alkyl side chains than the longer and bulkier F_6TCNNQ^-. However, the final amount of dopants at saturation in the layers of C_{12}-PBTTT is not related to their diffusion kinetics (vide infra).

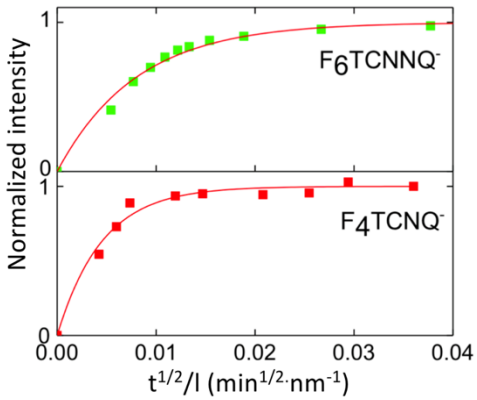

Figure 4. *A) Plot of normalized absorptions of both F_6TCNNQ (λ=1158 nm) and F_4TCNQ (λ=1158 nm) vs $t^{1/2}$/l to determine the diffusion coefficients* (1 mg/ml dopant solution in acetonitrile).

2.4. Angular distribution of dopant anions and polarons.

Angle-dependent polarized UV-Vis-NIR spectroscopy was used to further probe the degree of order and the distribution of the dopant anions in the oriented C_{12}-PBTTT matrix following the approach by Untilova et al. for F_4TCNQ-doped aligned P3HT.[26] The UV-Vis-NIR spectra were recorded for a variable polarization angle of the incident light with respect to the direction of rubbing in the 0° - 90° range (see figure ESI4C and ESI4D). On one side, comparing the angular distributions of the polaron band P1 and the original neutral polymer band of the pristine film highlights the impact of doping on in-plane alignment of the polymer chains. [15,24] On the other side, the comparison between the angular distributions of the anions and the polarons gives an indication on the correlations between dopant and polymer chain orientations. Such an analysis makes it possible to see if the dopant molecules are intercalated in the layer alkyl side chains in a random or highly ordered manner.

The plots of the absorbance of the neutral polymer, polarons and the dopant anions as a function of incident polarization angle are shown in Figure 5. The overlap of the anionic bands (873 nm for F_4TCNQ and 1158 nm for F_6TCNNQ) with the broad polaronic contribution made it difficult to

evaluate the true absorbance of the anions from the spectra directly. Hence, it was necessary to deconvolute the as-obtained spectra in order to extract the actual absorbance of the anions by subtracting the contribution from the polaron P2 (see figure ESI4). The angular dependences of the F_4TCNQ^- and F_6TCNNQ^- absorption bands after the subtraction of the P2 contribution are represented in figure 5A and B, respectively, whereas the angular dependences of the band amplitude versus angle are depicted in Figure 5C and D.

Table 1. Characteristics of angular distribution curves for the neutral polymer chains, the polaron and the anions in F_4TCNQ- and F_6TCNNQ-doped PBTTT C_{12} thin films.

Dopant	F_4TCNQ			F_6TCNNQ		
	C_{12}-PBTTT chains	F_4TCNQ^-	Polaron (P1)	C_{12}-PBTTT chains	F_6TCNNQ^-	Polaron (P1)
Dichroic ratio (D_R)	10.7	5.0	15	9.3	9.0	9.3
Order parameter (OP)	0.7	0.5	0.7	0.7	0.7	0.73

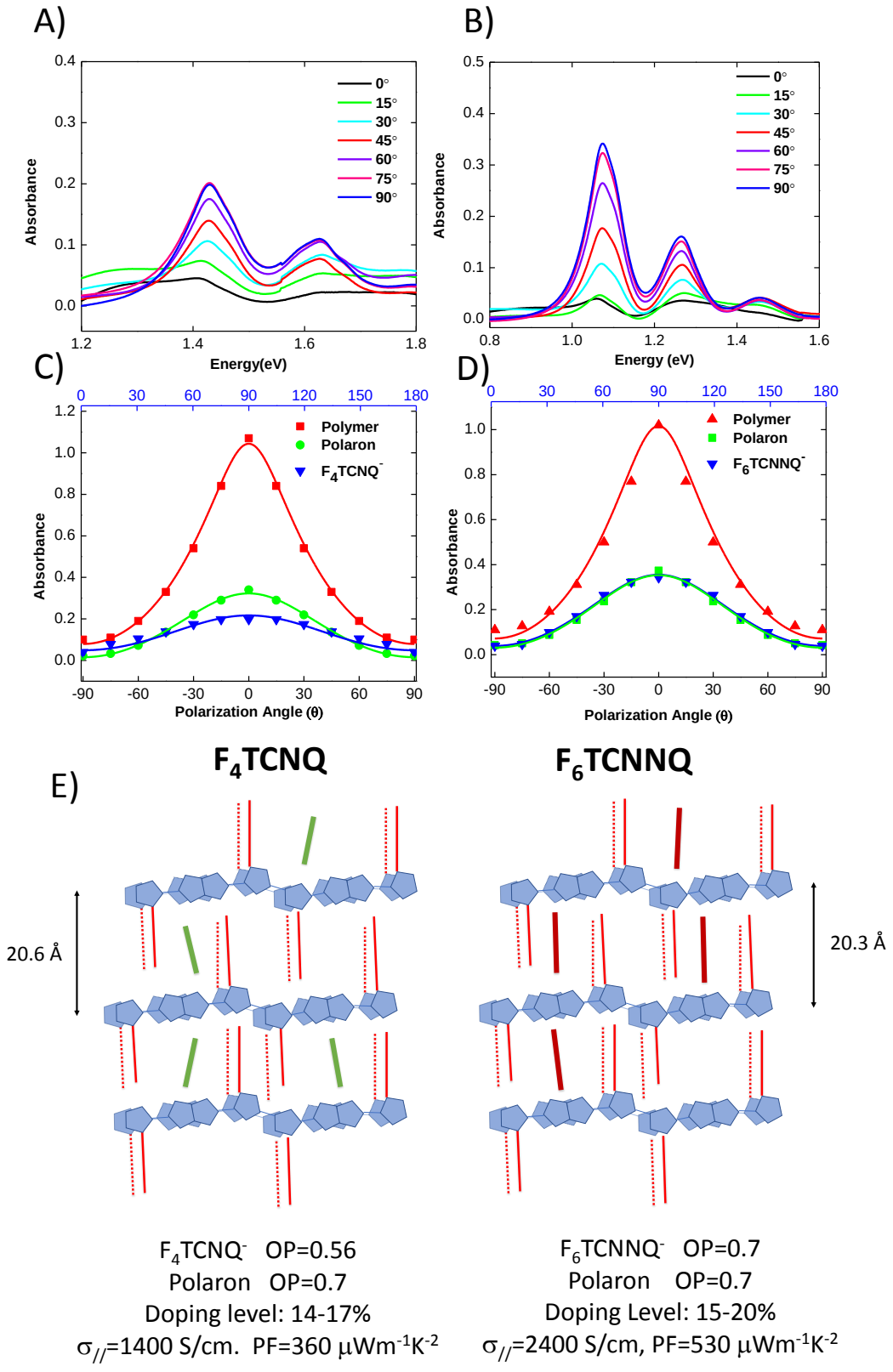

Figure 5. *Absorbance of the dopant anions after subtracting the background absorbance of the polaronic contribution P2 for A) F_4TCNQ^- and B) for F_6TCNNQ^-. C) Angular distribution of absorption*

bands of pristine C_{12}-PBTTT before doping, the F_4TCNQ^- anion (λ= 873nm) and the P1 band (λ= 2500 nm). D) Angular distribution of the absorption bands of oriented pristine C_{12}-PBTTT before doping, the F_6TCNNQ^- anion (λ= 1158 nm) and the polaronic P1 band (λ= 2500 nm). E) Schematic illustration of the dopant intercalation of F_4TCNQ and F_6TCNNQ in the layers of alkyl side chains of C_{12}-PBTTT and corresponding TE properties for films doped by ICD.

The dichroic ratio (DR) and 3D order parameters (OP) were used to quantify the degree of orientation of the neutral polymer, the polarons and the anions in the oriented C_{12}-PBTTT matrix. Table 1 collects the values of DR and OP for the films doped with F_4TCNQ and F_6TCNNQ.

The very small value of the absorption offset (A_0 = 0.07) before doping indicates that most of the chains are aligned and there is almost no contribution from a non-oriented fraction of C_{12}-PBTTT. The absorption offsets for both polarons and anions are also very small (≈ 0.05), which further confirms that the high degree of alignment of C_{12}-PBTTT is maintained after doping. In the case of F_4TCNQ doping, the calculated order parameters (OP) is 0.7 for the undoped C_{12}-PBTTT and 0.7 for the polarons. The similar values indicate that doping does not alter the alignment of the chains. The same observation was also obtained for the angular distribution measurements of F_4TCNQ-doped P3HT films.[15,26] In addition to this, the maximum of the angular distributions of both F_4TCNQ^- and F_6TCNNQ^- anions are clearly centered at 90°. This implies that the long axis of the dopants is indeed oriented around a plane orthogonal to the average polymer chain direction and not tilted.

Surprisingly, the order parameter calculated for the F_4TCNQ^- anions (0.56) is substantially lower as compared to that of the polarons (0.7). Similar trends were obtained in oriented P3HT films for the angular distribution of F_4TCNQ.[26] This suggests that the F_4TCNQ dopants are not strictly located in a plane orthogonal to the polymer chains, but are distributed around this average orientation.

The case of F_6TCNNQ doping is different. In that case, the polymer chains, polarons and the dopant F_6TCNNQ^- anions have a similar OP ≈ 0.7. This result supports the idea that, unlike F_4TCNQ^- anions, the long axis of F_6TCNNQ^- lies essentially in a plane that is perpendicular to the oriented C_{12}-PBTTT chains with little angular spread around this average orientation. In other words, the orientation of the F_6TCNNQ dopants is defined in a better way with respect to the polythiophene chains as compared to F_4TCNQ.

Why are F_6TCNNQ molecules better ordered in the layers of alkyl side chains than F_4TCNQ? To answer this question, we have used low-dose electron diffraction to probe the structure of the films as a function of doping concentration. As shown in our previous studies, doping results in the intercalation of dopant molecules in the layers of alkyl side chains as witnessed by the lattice expansion along the alkyl side chains and the contraction of the π-stacking periodicity.[8,10,15,31] Similarly, to the previous studies, we followed the structural changes in both F_4TCNQ and F_6TCNNQ doped C_{12}-PBTTT thin films and Figure 6 exemplifies the changes in the ED patterns upon doping (ICD protocol). The changes in d_{100} lattice periodicity are shown in figure H and G for F_4TCNQ and F_6TCNNQ, respectively.

Undoped C_{12}-PBTTT films prepared by high temperature rubbing show a sequence of h 0 0 (h= 1 - 4) reflections along the equatorial direction and no π-stacking (d_{020}) reflection. In addition, a strong 0 0 3 reflection is present along the rubbing direction, indicating that PBTTT crystals are mainly in face-on orientation (see figure 6 and ESI5). Doping with either F_4TCNQ or F_6TCNNQ does not modify to great extent the diffraction patterns and no change of contact plane or loss of in-plane orientation is observed upon doping. However, both d_{100} and d_{020} periodicities change with increasing doping concentration. Figure 6.G and 6.H depict the unit cell parameter variation as a function of dopant concentration for both ICD and DD methods for both F_4TCNQ and F_6TCNNQ-doped films.

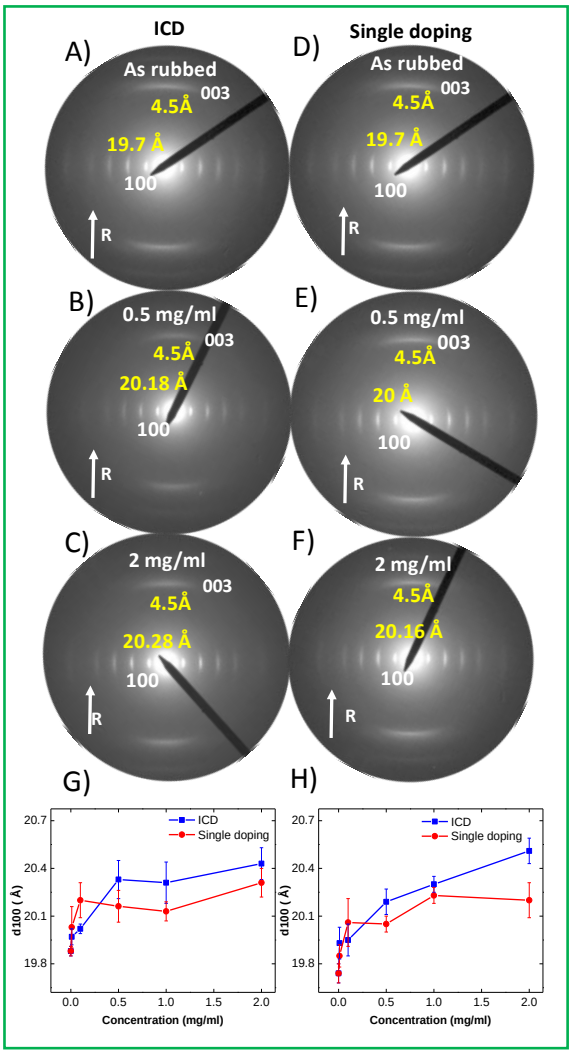

Figure 6. *Evolution of the electron diffraction patterns of F_6TCNNQ doped C_{12}-PBTTT (A-C) sequential addition (D-F) direct doping as a function of dopant concentration represent the rubbing direction Evolution of d_{100} spacing of the sequentially and directly doped C_{12}-PBTTT. G) Variation of d_{100} spacing of sequentially and directly doped F_6TCNNQ/C_{12}-PBTTT. H) Variation of d_{100} spacing of sequentially and directly doped F_4TCNQ/C_{12}-PBTTT. ICD at a concentration C means that the sample has been doped at all concentration steps below.*

For both dopants, an expansion along the side chain direction of the C_{12}-PBTTT unit cell is observed. For F_4TCNQ, a larger interlayer spacing variation from 19.7 Å up to 20.57 Å is evidenced than for

F_6TCNNQ, (from 19.7 Å to 20.28 Å). Surprisingly, the longer and bulkier F_6TCNNQ produces a smaller increase of d_{100} spacing up as compared to F_4TCNQ. Incidentally, the lattice expansion for both F_4TCNQ and F_6TCNNQ is significantly smaller with respect to $FeCl_3$ (d_{100} increases up to 23.7 Å). The lattice expansion in C_{12}-PBTTT is therefore not correlated to the dimensions of the dopants (F_4TCNQ has a long axis of 12 Å versus 14.4 Å for F_6TCNNQ). UV-Vis-NIR spectroscopy has shown that the doping level at saturation are 14% and 20% (dopant per thiophene cycle) for F_4TCNQ and F_6TCNNQ, respectively. Hence, the lower lattice expansion for F_6TCNNQ is not associated with a lower doping level.

Accordingly, TEM shows that doping C_{12}-PBTTT with F_6TCNNQ produces a smaller structural modification with respect to F_4TCNQ despite a larger dopant dimension and a higher doping level at saturation. Both these observations are counter-intuitive. Moreover, polarized UV-vis-NIR spectroscopy has shown that F_6TCNNQ dopants are better ordered in the side chain layers of C_{12}-PBTTT than F_4TCNQ. One element of response for these results is given by the study of the doping kinetics. Indeed, it has been shown that the diffusion coefficient of F_4TCNQ^- anions is larger than that of F_6TNNQ by a factor of 4-5. In other words, F_4TCNQ^- anions intercalates more rapidly in the lattice of C_{12}-PBTTT than F_6TCNNQ. This faster diffusion is possibly responsible for the more disordered distribution of F_4TCNQ dopants in the side chain layers of C_{12}-PBTTT. This fast F_4TCNQ intercalation may imply that the dopant molecules cannot find the optimal positions in the side chain layers. Accordingly, the C_{12}-PBTTT lattice expands more upon doping with F_4TCNQ than with F_6TCNNQ. Due to a slower diffusion in C_{12}-PBTTT, F_6TCNNQ^- molecules can find the best position in the side chain lattice, causing a smaller lattice expansion despite their larger molecular dimension (long axis of 1.47 nm for F_6TCNNQ versus 1.1 nm for F_4TCNQ). Preservation of pristine order in C_{12}-PBTTT films upon doping with F_6TCNNQ is also supported by the fact that the polaronic bands are more red-shifted for F_6TCNNQ than for F_4TCNQ. Overall, these results indicate that the control of doping kinetics is possibly a means to produce doped PSC films with enhanced structural perfection. This was an incentive to study the impact of the doping method on the TE properties of aligned C_{12}-PBTTT films.

In particular, it is shown that a progressive intercalation of dopants can produce films with superior TE performances.

2.5. Influence of the method of sequential doping on the charge conductivity.

Two different procedures were used to dope the oriented films i.e. incremental concentration doping (ICD) and direct doping (DD) (see Figure 1). In ICD, each sample is doped by dipping it successively in the solutions of dopants of increasing concentration up to a given concentration while in the direct doping procedure, each sample is dipped a single time in a solution of a given concentration. Typically for ICD, we consider the doping in successive solutions of 0.01, 0.1, 0.5, 1, 2 and 5 mg/ml. ICD at a concentration C means that the sample has been doped at all concentration steps below. For instance ICD at 1.0 mg/ml means that the sample has been doped successively at 0.01, 0.1 and 0.5 mg/mL).

Figure 7 shows the evolution of the charge conductivity, Seebeck coefficient and power factors for oriented C_{12}-PBTTT films as a function of doping concentration for F_4TCNQ and F_6TCNNQ.

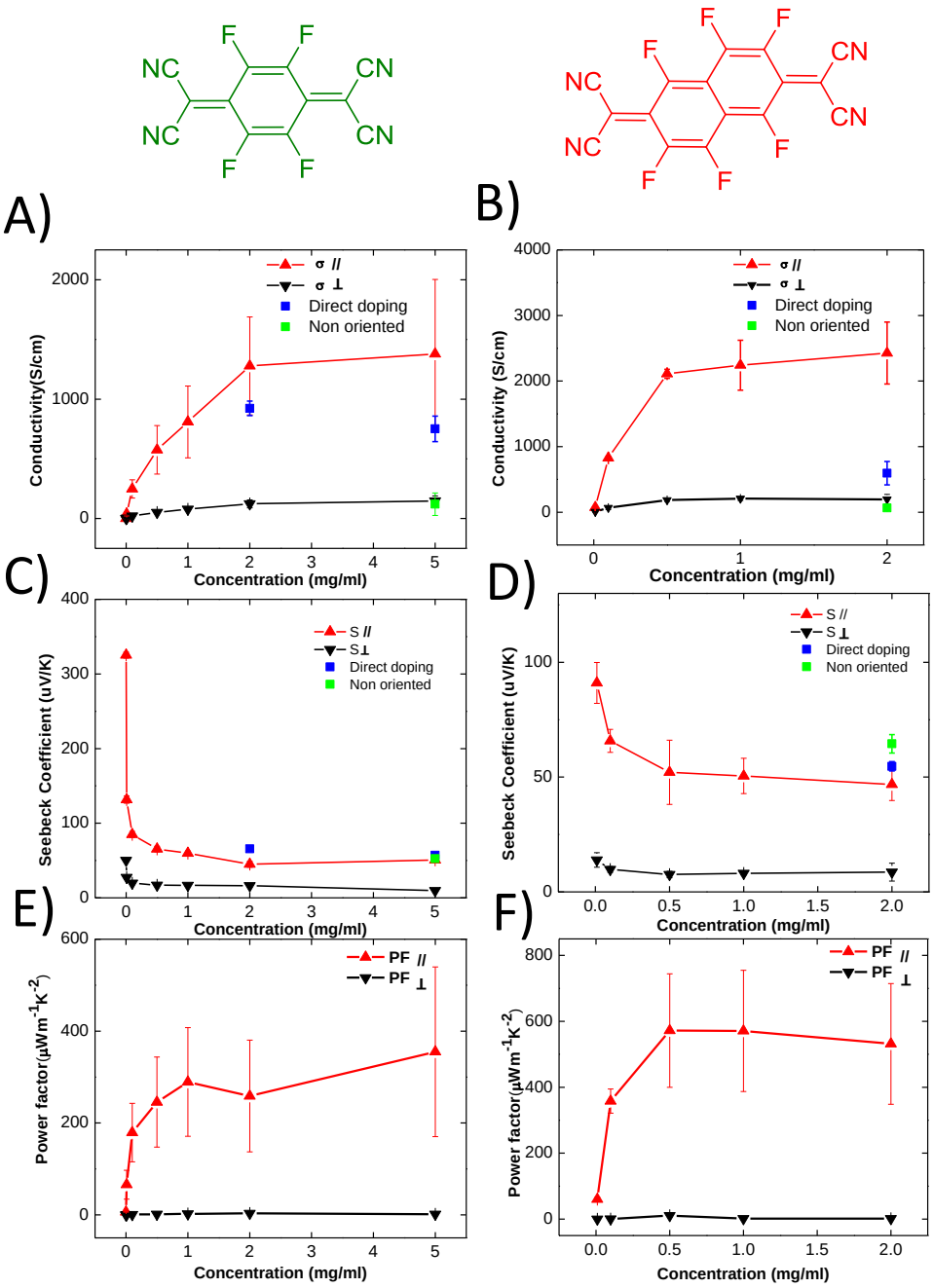

Figure 7. *Evolution of the charge conductivity (A and B) and of the Seebeck coefficient (C and D) in oriented films of C_{12}-PBTTT as a function of increasing doping concentration of F_4TCNQ and F_6TCNNQ, respectively. The curves correspond to one sample doped by incremental increase of doping concentration (ICD). Each value of conductivity and Seebeck coefficient for a given concentration corresponds to the value after doping the sample successively at all lower doping concentrations. Both S and σ are measured parallel (red) and perpendicular (black) to the rubbing directions. For comparison, we also show the values of samples obtained for direct doping at high doping*

concentration (2 and 5 mg/ml for F_4TCNQ and 5 mg/ml for F_6TCNNQ) in parallel direction. The conductivity of non-oriented samples was also measured at maximum doping concentration using the ICD method. E) and F) Evolution of the power factor as a function of increasing doping concentration of F_4TCNQ and F_6TCNNQ doped films of C_{12}-PBTTT, respectively. Films were oriented by high temperature rubbing at 125°C and doped by incremental concentration doping.

As observed previously, the doping of all oriented thin films produces higher electrical conductivity along the rubbing direction than perpendicular to it (see Figure 7). [14–16,26] The conductivity in the direction perpendicular to the rubbing at saturation is close to that of non-oriented thin films (65±4 S/cm for F_6TCNNQ and 120±94 S/cm for F_4TCNQ).

Incremental doping on the same device results in higher electrical conductivities as compared to direct doping. ICD with F_4TCNQ leads to a very high electrical conductivity of $\sigma_{//}$= 1380±700 S/cm along the rubbing direction *versus* $\sigma_{//}$=920±60 S/cm for the same film doped by DD. Hence, ICD produced 1.5 times higher electrical conductivity than direct doping in the case of F_4TCNQ. The trend is even more pronounced for F_6TCNNQ: $\sigma_{//}$=2430±500 S/cm for ICD (2mg/ml) *versus* $\sigma_{//}$=600±200 S/cm for DD. The electrical conductivities measured perpendicular to the rubbing direction are similar to those observed for the non-oriented films of C_{12}-PBTTT). This further confirms that the lower electrical conductivity in non-oriented samples is limited by the poor transport perpendicular to the polymer chains.

The larger charge conductivity observed in samples doped by ICD can be either a consequence of a higher doping level leading to a higher charge carrier density or to a higher charge mobility. Therefore, an oriented C_{12}-PBTTT thin film was dipped 4 times in pure ACN before direct doping (2 mg/ml of F_6TCNNQ in acetonitrile) (4ACN+DD) and its UV-vis-NIR spectra was compared with that of the film doped by ICD (the reason for the dipping of the films in pure ACN was to rule out a possible influence of the solvent on the film structure). As seen in figure ESI5, the polarized UV-Vis-NIR of both ICD and 4ACN+DD films show the same intensities of polaronic bands P1 and P2 and almost

similar contributions from the neutral polymer. This implies that doping levels are quite similar for ICD and 4ACN+DD samples and cannot explain the large difference in conductivity observed for ICD and DD. Moreover, as seen from Table 2, the 4ACN+DD sample shows a lower conductivity as compared to the ICD sample, indicating that dipping in ACN does not explain the observed conductivity enhancement seen for ICD. Hence, ICD and DD produce similar charge carrier densities and the observed higher electrical conductivities for ICD might be related to a difference in the charge carrier mobility.

TEM was accordingly used to evaluate the impact of doping method on the film structure that determines charge mobility. Figure ESI6 compares the evolution of the ED patterns of C_{12}-PBTTT films doped by ICD and DD for different doping concentrations of F_4TCNQ. Overall, no clear differences in the intensities or the width of the reflections are evidenced. Order along the chain direction, side chains and π-stacking are preserved for both doping protocols. To highlight differences, it is necessary to look more carefully at the variation of d_{100} and d_{020} lattice spacing versus doping concentration (figure 6.G and 6.H). For both dopants, ICD leads to a larger interlayer spacing variation as compared to DD (F_4TCNQ: 20.57 Å for ICD *versus* 20.27 Å for DD; F_6TCNNQ: 20.28 Å for ICD *versus* 20.16 Å for DD). For both dopants, the lattice expansion becomes larger for ICD than DD for doping concentrations beyond 0.5 mg/ml. These observations demonstrate that ICD and DD produce C_{12}-PBTTT films with rather similar structures and very subtle differences in lattice expansion along the alkyl side chains and contraction in the π-stacking direction. These observed differences in structure may account, at least in part, for the difference in charge transport between ICD and DD. As an alternative, it might be that the differences in charge conductivity between DD and ICD are related to differences in the doping of the amorphous phase that is not probed by electron diffraction.

2.6. Influence of doping method on Seebeck coefficients and power factors.

Seebeck coefficients were also anisotropic and higher Seebeck coefficients were measured along the rubbing direction for both F_4TCNQ and F_6TCNNQ doped C_{12}-PBTTT. The values of the Seebeck coefficients were little affected by the doping method. For instance, ICD with F_4TCNQ (5 mg/ml) leads to $S_{//}$= 51±4 µV/K while for DD $S_{//}$= 57±3 µV/K (see figure 7.C and D). This difference is consistent with the higher conductivity seen for ICD *versus* DD. Similarly, ICD with F_6TCNNQ (2 mg/ml) leads to $S_{//}$=47±3 µV/K *versus* 64.5±3 µV/K for DD at the same concentration. It is worth to mention that the Seebeck coefficients of non-oriented samples were similar to the values measured along the chain direction (53±3 µV/K for F_4TCNQ and 65±4 µV/K for F_6TCNNQ), indicating that alignment is not detrimental for the Seebeck coefficient while it is highly beneficial to enhance charge conductivity.

As expected, the increase of electrical conductivity in oriented C_{12}-PBTTT thin films enhances the power factors along the chain direction. Incremental concentration doping (ICD) of C_{12}-PBTTT films with F_4TCNQ and F_6TCNNQ produced high power factors of 355±200 $\mu W m^{-1} K^{-2}$ and 530±200 $\mu W m^{-1} K^{-2}$, respectively. For comparison, a very high PF of 1900 $\mu W \cdot m^{-1} \cdot K^{-2}$ was obtained for $FeCl_3$-doped C_{12}-PBTTT. [15] As expected, ICD provided higher power factors than DD for both F_4TCNQ and F_6TCNNQ. The poor electrical conductivities of the non-oriented C_{12}-PBTTT thin film lead to a PF that is lower by more than one order of magnitude compared to the aligned films: only 33 $\mu W \cdot m^{-1} \cdot K^{-2}$ for F_4TCNQ and 27±3 $\mu W \cdot m^{-1} \cdot K^{-2}$ for F_6TCNNQ. The dependence of PF with doping concentration (figure 6) shows the same characteristic increase and saturation for concentrations in the range 2-5 mg/ml for both dopants.

Table 2. *Summary of maximum electrical conductivities, Seebeck coefficient and power factors observed upon incremental and single doping methods.DD: direct doping. ICD: Incremental Concentration Doping.*

Dopant	Doping method	σ (S/cm)	S (μV/K)	PF $\mu Wm^{-1}K^{-2}$
F_6TCNNQ	ICD	2430±500	47±7	530±200
	DD	600±200	64.5±3	247±74
	4ACN+DD	970±200	55±1	293±63
F_4TCNQ	ICD	1380±700	50.7±4	355±200
	DD	920±60	57±3	300±20
	Vapor Phase*	670	42	120

2.7. Correlations between Seebeck coefficient and charge conductivity in oriented thin films.

The ICD method is particularly useful to probe S-σ correlations because a single sample of well-defined initial structure and orientation is progressively doped at higher dopant concentration, which alleviates all issues related to sample-to-sample statistics due to structural variations. In the previous publications,[15,16] we have demonstrated that the S-σ correlation is well described as proposed by Chabinyc[4] and co-workers by the relation $S_{//} \propto \sigma_{//}^{-1/4}$ for F_4TCNQ and $FeCl_3$ dopants in the direction parallel to the polymer chains. In oriented samples, we have observed a different correlation in the direction perpendicular to the backbone, namely $S_{\perp} \propto -\ln(\sigma_{\perp})$. The open question relative to these correlations is whether or not they depend on the chemical nature of the dopant.

This is why we collected all S,σ data for films doped by ICD with the dopants F_4TCNQ, F_6TCNNQ and $FeCl_3$ (data recovered from our previously reported study) [15] on the same plot (see Figure 8). The correlations were plotted for both parallel and perpendicular orientations with respect to the chain direction.

It is remarkable to see that all the data points align on the same master curves over 5 decades of charge conductivity, regardless of the dopant and for both directions parallel and perpendicular to the C_{12}-PBTTT chains. *This demonstrates that the S-σ correlation in C_{12}-PBTTT is not dependent on the chemical nature of the dopant but mainly on the packing and electronic structure of the oxidized polymer.* Accordingly, this correlation is characteristic of the charge transport of the polymer C_{12}-PBTTT as long as its structure is marginally modified upon dopant intercalation during ICD. The only notable difference related to the dopants is the limit in conductivity that is reached for each dopant. This limit correlates with the maximum doping/oxidation levels reached for each dopant that follows the sequence $F_4TCNQ<F_6TCNNQ<FeCl_3$.

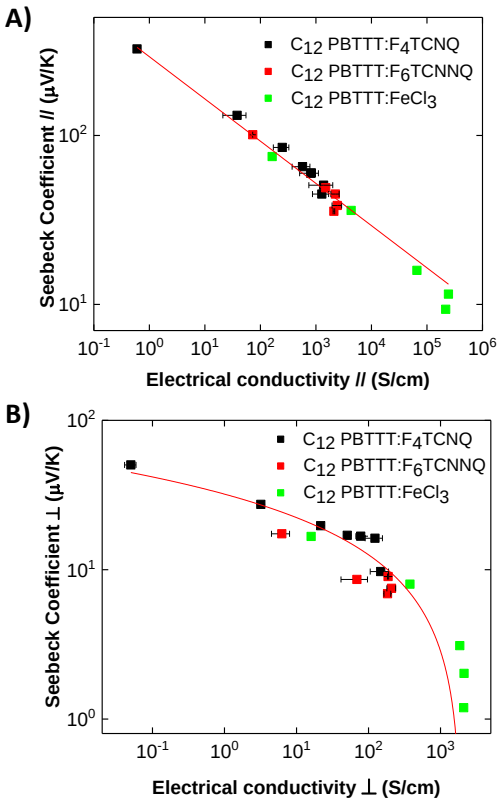

Figure 8. *Correlation between Seebeck coefficient S and electrical conductivity σ in highly oriented thin films of C_{12}-PBTTT (T_R=125°C) doped with F_4TCNQ (black squares), F_6TCNNQ (red squares) and $FeCl_3$ (green squares). The full lines correspond to the results of the fit using the scaling laws $S_{//} \propto \sigma_{//}^{-1/4}$ and $S_{\perp} \propto -\ln(\sigma_{\perp})$.*

In a recent work by Scheunemann et al, the impact of structural anisotropy on the thermoelectric properties of organic semiconductors was analyzed by kinetic Monte Carlo simulations. [32] The difference in the S versus σ correlations along and perpendicular to the rubbing is explained by introducing an anisotropic localization length of the carriers (larger in the direction of chain orientation). The anisotropy in S and σ is found to correlate with the anisotropy in localization length. The simulations show that, in the direction perpendicular to the chains, the thermopower follows a universal curve *versus* σ that is independent of the dopant and polymer side chain. In strong contrast, along the chain direction, a different trend is observed and a dependence with the length of the alkyl side chains has been evidenced. [32] While most studies have reported the $S \propto \sigma^{-}$

$^{1/4}$ power law, a recent work by Tanaka et al. reported a departure from this law for non-oriented PBTTT doped by the electrolyte-gating technique when high charge conductivities beyond 10^2 S/cm are reached. [33] This result can be understood by the fact that the S vs σ relation in non-oriented PBTTT is dominated by the transport phenomena perpendicular to the side chains of the polymer. This is why the observations by Tanaka et al. are similar to the ones reported in this study for $S_{\perp}$ and $\sigma_{\perp}$. Only for highly aligned PBTTT films is it possible to evidence the intrinsic S vs σ correlation along the chain direction.

3. Conclusion.

A combination of Polarized UV-Vis-NIR spectroscopy and electron diffraction is used to uncover various characteristics of the doping of C_{12}-PBTTT with F_4TCNQ and F_6TCNNQ. F_6TCNNQ^- anion are better ordered in the layers of alkyl side chains and lie in a plane strictly perpendicular to the C_{12}-PBTTT backbone whereas F_4TCNQ^- anions are more distributed around this direction. The better ordering of F_6TCNNQ in the layers of alkyl side chains of C_{12}-PBTTT is attributed to the slower diffusion of this molecule as compared to F_4TCNNQ. Similarly to rr-P3HT, doping C_{12}-PBTTT with F_6TCNNQ and F_4TCNQ produces an expansion of the unit cell along the d_{100} and a compression along the π stacking direction. However, the extent of lattice expansion along the alkyl side chains is not correlated to the length of the dopant's long axis.

In addition, a new doping protocol called incremental concentration doping (ICD) is proposed. Doping a C_{12}-PBTTT film with solutions of increasing dopant concentration leads to higher electrical conductivities and higher power factors than direct doping. The enhanced TE properties achieved by ICD are attributed to the preservation of pristine order and higher resulting carrier mobilities. The degree of ordering of the dopant anion in the alkyl side chain layers is an important factor that determines the resulting TE performances of the doped polymer. From that perspective, it would be instructive to determine the ordering of dopants in the polymer matrix when doped from the vapor phase since such doping leads usually to higher TE performances. The determination of the angular-

dependence of the anion and polaronic bands via polarized UV-vis-NIR spectroscopy on oriented polymer films is an elegant methodology to address this issue. Preliminary results further demonstrate that ICD is a versatile method that can be applied to other polymers such as P3HT and other dopants ($FeCl_3$) to reach better thermoelectric performances. Using the ICD method at higher temperatures might be a further means to enhance the thermoelectric performances of such aligned thin films.

4. Experimental section.

a) Orientation and doping of thin films: C_{12}-PBTTT was synthesized following the procedure described in the literature and in our previous work (M_w = 26 kDa, PDI = 1.73). [24]

F_6TCNNQ was synthesized following the general method given in the SI. F_4TCNQ was purchased from TCI. Anhydrous solvents such as acetonitrile and *ortho*-dichlorobenzene were obtained from Sigma-Aldrich and used without purification.

The C_{12}-PBTTT films were prepared by doctor-blading a solution of P3HT in *ortho*-dichlorobenzene (10 mg mL^{-1}) at 160°C on glass slide substrates pre-covered with a sacrificial hydrosoluble NaPSS (10 mg mL^{-1} aq) layer. The orientation of the films by high temperature-rubbing followed the protocol described in previous publications.[24,26] Oriented polymer films were prepared by using a homemade set up consisting of a translating hot plate on which the sample is fixed and a rotating cylinder covered with a microfiber cloth. The films were rubbed at different rubbing temperatures. To determine the film thickness after rubbing, the films were melt-annealed to randomize the in-plane chain direction and the thickness was extracted from the UV-vis absorbance.

The doping was performed following the sequential doping method with full sample immersion for 10 s in the dopant solution at a constant concentration of 1 mg mL^{-1} in anhydrous

acetonitrile.[9] No rinsing step was conducted. Doping as well as rubbing were performed under nitrogen atmosphere.

b) Structural analysis by TEM. Oriented areas were identified for TEM analysis by optical microscopy (Leica DMR-X microscope). For TEM investigations, the oriented C_{12}-PBTTT thin films prepared on NaPSS by high temperature rubbing were carbon-coated and the films were recovered on copper TEM grids by floating on water. The TEM grids were doped by ICD using dopant solutions (F_4TCNQ or F_6TCNNQ) in acetonitrile in the glove box. The dopant solution was allowed to stay on the TEM grid for 20-30 s and the excess solution was removed by blotting. The structural variation in the doped thin films was followed by electron diffraction using a transmission electron microscope. In the direct doping method, carbon-coated TEM grids were doped directly at a given concentration of dopants. In the case of ICD, the grids were doped by dipping in solutions of increasing concentration up to the desired concentration.

TEM was performed in bright field and diffraction modes using a CM12 Philips microscope equipped with a MVIII (Soft Imaging System) charge coupled device camera. Calibration of the reticular distances in the ED patterns was made with an oriented polytetrafluoroethylene (PTFE) film. Beam exposure was set to a minimum using the low dose system to avoid dedoping under the electron beam that is observed when the same zone is exposed for a prolonged period of time.

c) Polarized UV–Vis–NIR absorption. A Varian Cary 5000 spectrometer with polarized incident light and spectral resolution of 1 nm was used to measure the polarized UV–vis–NIR absorption (350–2500 nm) of the doped films. For all polarized UV-vis-NIR measurements, the C_{12}-PBTTT/NaPSS/glass films are used without floating. Alignment of pristine and doped polymer films was quantified by the dichroic ration DR and the 3D order parameter OP following the equations :

$$DR = \frac{Abs//}{Abs\perp} \quad (2)$$

$$OP = \frac{DR-1}{DR+2} \quad (3)$$

Where $Abs_{//}$ is the absorption parallel to the rubbing and $Abs_{\perp}$ is the absorption perpendicular to the rubbing direction. DR is the dichroic ratio.

The angular distributions of the absorption for the polarons, F_4TCNQ^- and F_6TCNNQ^- anions in oriented C_{12}-PBTTT are fitted following the same procedure as described in reference 28. In particular, we used the following equations: [26]

$$A(\lambda,\theta) = A_0 - \log\left[1 - \frac{\beta}{\beta+1}(1 + 3cos2\theta)\right] \qquad (4)$$

Where,

$$\beta = \frac{1}{3}\tanh(\Delta A \frac{ln10}{2}) \qquad (5)$$

Here A_0 is the un-polarized offset absorption related to the non-aligned fraction of C_{12}-PBTTT and $\Delta A = A_{max} - A_{min}$, Amax (0°, //) and A_{min} (90°, $\perp$) for P1 and A_{max} (90°, $\perp$) and A_{min} (0°, //) for both F_4TCNQ^- and F_6TCNNQ^-.

The apparent doping level is calculated as proposed in references 15 and 26 using the ratio $C_{anion}/C_{thiophene}$, where C_{anion} and $C_{thiophene}$ are the molar concentrations of thiophenes and dopant anions, respectively. $C_{thiophene}$ is calculated from the unit cell parameters of the doped PBTTT phase and from the fact that the unit cell hosts 8 thiophene rings. Thus $C_{thiophene} = \frac{8}{V}$ where V - is the volume of the doped unit cell. The dopant anion concentration was calculated from the Beer-Lambert-Bouguer law:

$$A = \varepsilon_{anion} \cdot l \cdot C_{anion}$$

where A - is the absorbance of the anion, ε - the extinction coefficient of the anion, l - the film thickness and, C_{anion}-the molar concentration of the anion. The extinction coefficients for F_4TCNQ and F_6TCNNQ are 50000 $l \cdot Mol^{-1} \cdot cm^{-1}$ and 53700 $l \cdot Mol^{-1} \cdot cm^{-1}$ (reference 14 and figure ESI1)

d) Charge conductivity and Seebeck coefficient. The detailed device preparation method is described in ref 14. All devices were fabricated on glass substrates, cleaned by ultrasonication in acetone, ethanol, Hellmanex and deionized water (x3 times). The cleaned substrates were dried under nitrogen and exposed to plasma prior to film deposition. Gold electrical contacts (40 nm thick) in a four-points probe geometry (1 mm spacing between electrodes, 5 mm length) were evaporated through a shadow mask (rate of 4–6 Å/s) after deposition of a first layer of chromium (2.5 nm thick) (evaporation rate 0.5–1 Å/s).

The geometry of deposited gold electrodes allows determining the charge transport and thermopower on a same substrate in both parallel and perpendicular directions to rubbing (see Figure S3 reference 14). Oriented films of P3HT were floated on distilled water and carefully recovered on the device with pre-deposited gold electrodes. After float-off, the samples are left for drying 1hr in ambient and then transferred in the glovebox via the transfer chamber under primary vacuum (pumping for several minutes). Doping using DD or ICD methods were performed on the polymer/device samples in a glovebox (Jacomex). Four-point probe measurements of electrical conductivity were performed using a Keithley 4200-SCS and a Lab Assistant Semiprobe station under N_2 atmosphere. To derive the resistivity ρ from the sheet resistance R measured on the device, the geometrical correction factor C was first determined such that $\rho = R.C.t$ where t is the film thickness. The geometrical correction factor C was determined for four-line electrode geometry by measuring the sheet resistance on the same sample using a classical four-point apparatus and the four-line electrode device , yielding C = 1.81. The average conductivity value for a given rubbing temperature was taken as the average of two to four devices.

Thermopower measurements were conducted in nitrogen atmosphere on the same devices. The thermopower was measured using a differential temperature method whereby a temperature gradient is established across the sample along or perpendicular to the rubbing direction. The details of the experimental setup are given in reference 14.

Acknowledgements

Bernard Lotz is acknowledged for careful reading of the manuscript. We thank Christian Blanck and Marc Schmutz for technical support in TEM. We thank Nicolas Zimmermann for the preparation of the pre-patterned devices (gold deposition). MB is grateful for the financial supports from the ANR Anisotherm (ANR-17-CE05-0012) and CNRS grant PEPS Thermobody. Viktoriia Untilova is grateful for financial support from IRTG Softmatter / Région Grand'Est.

Conflicts of interests.

The authors declare no conflict of interest.

Supporting Information

The Supporting Information is available free of charge.

References

[1] O. Bubnova, Z. U. Khan, A. Malti, S. Braun, M. Fahlman, M. Berggren, X. Crispin, *Nature Materials* 2011, ***10***, 429.

[2] O. Bubnova and X. Crispin, *Energy Environ. Sci.* 2012, ***5***, 9345.

[3] K.-H. Yim, G. L. Whiting, C. E. Murphy, J. J. M. Halls, J. H. Burroughes, R. H. Friend, J.-S. Kim, *Advanced Materials* 2008, ***20***, 3319.

[4] A. M. Glaudell, J. E. Cochran, S. N. Patel and M. L. Chabinyc, *Advanced Energy Materials* 2015, **5**, 1401072.

[5] D. Kiefer, L. Yu, E. Fransson, A. Gómez, D. Primetzhofer, A. Amassian, M. Campoy-Quiles, C. Müller, *Adv. Sci.* 2017, **4**, 1600203.

[6] D. T. Duong, C. Wang, E. Antono, M. F. Toney and A. Salleo, *Organic Electronics*, 2013, **14**, 1330–1336.

[7] C. Y. Kao, B. Lee, L. S. Wielunski, M. Heeney, I. McCulloch, E. Garfunkel, L. C. Feldman, V. Podzorov, *Advanced Functional Materials* 2009, **19**, 1906.

[8] S. N. Patel, A. M. Glaudell, K. A. Peterson, E. M. Thomas, K. A. O'Hara, E. Lim and M. L. Chabinyc, *Sci Adv*, 2017, **3**, e1700434.

[9] D. T. Scholes, S. A. Hawks, P. Y. Yee, H. Wu, J. R. Lindemuth, S. H. Tolbert, B. J. Schwartz, *J. Phys. Chem. Lett.* 2015, **6**, 4786.

[10] D. T. Scholes, P. Y. Yee, J. R. Lindemuth, H. Kang, J. Onorato, R. Ghosh, C. K. Luscombe, F. C. Spano, S. H. Tolbert and B. J. Schwartz, *Advanced Functional Materials* 2017, **27**, 1702654.

[11] J. E. Cochran, M. J. N. Junk, A. M. Glaudell, P. L. Miller, J. S. Cowart, M. F. Toney, C. J. Hawker, B. F. Chmelka, M. L. Chabinyc, *Macromolecules* 2014, **47**, 6836.

[12] J. Hynynen, D. Kiefer, L. Yu, R. Kroon, R. Munir, A. Amassian, M. Kemerink, C. Müller, *Macromolecules* 2017, **50**, 8140.

[13] I. E. Jacobs, E. W. Aasen, J. L. Oliveira, T. N. Fonseca, J. D. Roehling, J. Li, G. Zhang, M. P. Augustine, M. Mascal and A. J. Moule, *J. Mater. Chem. C* 2016, **4**, 3454–3466.

[14] A. Hamidi-Sakr, L. Biniek, J.-L. Bantignies, D. Maurin, L. Herrmann, N. Leclerc, P. Lévêque, V. Vijayakumar, N. Zimmermann and M. Brinkmann, *Advanced Functional Materials* 2017, **27**, 1700173.

[15] V. Vijayakumar, Y. Zhong, V. Untilova, M. Bahri, L. Herrmann, L. Biniek, N. Leclerc and M. Brinkmann, *Advanced Energy Materials*, 2019, **9**, 1900266.

[16] V. Vijayakumar, E. Zaborova, L. Biniek, H. Zeng, L. Herrmann, A. Carvalho, O. Boyron, N. Leclerc and M. Brinkmann, *ACS Appl. Mater. Interfaces* 2019, **11**, 4942.

[17] K. Tashiro, M. Kobayashi, T. Kawai and K. Yoshino, *Polymer* 1997, **38**, 2867.

[18] J. Yamamoto and Y.Furukawa, *J. Phys. Chem. B* 2015, **119**, 4788.

[19] Z. Liang, Y. Zhang, M. Souri, X. Luo, A. M. Boehm, R. Li, Y. Zhang, T. Wang, D.-Y. Kim, J. Mei, S.-R. Marder and K.-R. Graham, *J. Mater. Chem. A* 2018, **6**, 16495.

[20] B. Yurash, D. X. Cao, V. V. Brus, D. Leifert, M. Wang, A. Dixon, M. Seifrid, A. E. Mansour, D. Lungwitz, T. Liu, P. J. Santiago, K. R. Graham, N. Koch, G. C. Bazan and T.-Q. Nguyen, *Nature Materials* 2019, **18**, 1327.

[21] P. K. Koech, A. B. Padmaperuma, L. Wang, J. S. Swensen, E. Polikarpov, J. T. Darsell, J. E. Rainbolt, D. J. Gaspar, *Chem. Mater.* 2010, **22**, 3926.

[22] Y. Karpov, T. Erdmann, M. Stamm, U. Lappan, O. Guskova, M. Malanin, I. Raguzin, T. Beryozkina, V. Bakulev, F. Günther, S. Gemming, G. Seifert, M. Hambsch, S. Mannsfeld, B. Voit, A. Kiriy, *Macromolecules* 2017, ***50***, 914.

[23] P. Pingel and D. Neher, *Phys. Rev. B* 2013, **87**, 115209.

[24] L. Biniek, N. Leclerc, T. Heiser, R. Bechara and M. Brinkmann, *Macromolecules* 2013, **46**, 4014-4023.

[25] L. Biniek, S. Pouget, D. Djurado, E. Gonthier, K. Tremel, N. Kayunkid, E. Zaborova, N. Crespo-Monteiro, O. Boyron, N. Leclerc, S. Ludwigs and M. Brinkmann, *Macromolecules* 2014, **47**, 3871.

[26] V. Untilova, T. Biskup, L. Biniek, V. Vijayakumar and M. Brinkmann, Macromolecules, 2020, **53**, 2441.

[27] R. Ghosh, C. M. Pochas and F. C. Spano, *J. Phys. Chem. C* 2016, **120**, 11394.

[28] R. Ghosh, A. R. Chew, J. Onorato, V. Pakhnyuk, C. K. Luscombe, A. Salleo and F. C. Spano, *J. Phys. Chem. C* 2018, **122**, 18048.

[29] J. Li, C. Koshnick, S. O. Diallo, S. Ackling, D. M. Huang, I. E. Jacobs, T. F. Harrelson, K. Hong, G. Zhang, J. Beckett, M. Mascal and A. J. Moulé, *Macromolecules*, 2017, **50**, 5476–5489.

[30] A. J. Maliakal, *ACS Appl. Mater. Interfaces* 2013, **5**, 8300.

[31] R. Sata, H. Suzuki, N. Ueno, Y. Morisawa, M. Hatanaka and T. Wakabayashia, *J. Chem. Phys.*

2019, **32**, 175.

[32] D. Scheunemann, V. Vijayakumar, H. Zheng, P. Durand, N. Leclerc, M. Brinkmann and M. Kemmerink, *Advanced Electronic Materials* 2020, **6**, 20000218.

[33] H. Tanaka, K. Kanahashi, N. Takekoshi, H. Mada, H. Ito, Y. Shimoi, H. Ohta and T. Takenobu, *Sci. Adv.* 2020, **6**, eaay8065.